

Electronic Supplementary Information

Reversible low-temperature redox activity and selective oxidation catalysis derived from concerted activation of multiple metal species on Cr and Rh-incorporated ceria catalysts

Satoru Ikemoto,^a Xiubing Huang,^b Satoshi Muratsugu,^{*a,c} Shoko Nagase,^a Takanori Koitaya,^{c,d} Hirotsuke Matsui,^a Gen-ichi Yokota,^a Takatoshi Sudoh,^a Ayako Hashimoto,^{c,e} Yuanyuan Tan,^b Susumu Yamamoto,^f Jiayi Tang,^g Iwao Matsuda,^f Jun Yoshinobu,^f Toshihiko Yokoyama,^d Shinpei Kusaka,^h Ryotaro Matsuda,^h and Mizuki Tada^{*a,b}

^a Department of Chemistry, Graduate School of Science, Nagoya University, Furo-cho, Chikusa-ku, Nagoya, Aichi 464-8602, Japan.

^b Research Center for Materials Science (RCMS) & Integrated Research Consortium on Chemical Science (IRCCS), Nagoya University, Furo-cho, Chikusa-ku, Nagoya, Aichi 464-8602, Japan.

^c Japan Science and Technology Agency (JST), Precursory Research for Embryonic Science and Technology (PRESTO), 4-1-8 Honcho, Kawaguchi 332-0012, Japan.

^d Department of Materials Molecular Science, Institute for Molecular Science, Myodaiji-cho, Okazaki, Aichi 444-8585, Japan.

^e In-situ Characterization Technique Development Group, National Institute for Materials Science, 1-2-1 Sengen, Tsukuba 305-0047, Japan.

^f The Institute for Solid State Physics, The University of Tokyo, 5-1-5, Kashiwanoha, Kashiwa, Chiba 277-8581, Japan.

^g Graduate School of Engineering, University of Hyogo, 2167, Shosha, Himeji, Hyogo 671-2280, Japan.

^h Department of Chemistry and Biotechnology, Graduate School of Engineering, Nagoya University, Furo-cho, Chikusa-ku, Nagoya, Aichi 464-8602, Japan.

Table of Contents

Details for catalyst characterization	S3
Table S1. Catalytic Performances for 1-Octanol Oxidation	S5
Table S2. Catalytic Performances of $\text{Cr}_{0.19}\text{Rh}_{0.06}\text{CeO}_z$ for the Selective Oxidation of Alcohols	S6
Table S3. Structural Parameters Obtained by Curve-Fitting Analysis of Rh K-edge EXAFS for $\text{Cr}_{0.19}\text{Rh}_{0.06}\text{CeO}_z$	S7
Table S4. Parameters for <i>In Situ</i> QXAFS Measurements	S7
Fig. S1. TEM images of $\text{Cr}_{0.19}\text{Rh}_{0.06}\text{CeO}_z$.	S8
Fig. S2. HAADF-STEM-EDS images of $\text{Cr}_{0.19}\text{Rh}_{0.06}\text{CeO}_z$.	S9
Fig. S3. HAADF-STEM-EELS images of $\text{Cr}_{0.19}\text{Rh}_{0.06}\text{CeO}_z$.	S10
Fig. S4. (A) Cr K-edge, (B) Rh K-edge, and (C) Ce L _{III} -edge XANES spectra of $\text{Cr}_{0.19}\text{Rh}_{0.06}\text{CeO}_z$ with standard samples.	S11
Fig. S5. (A) Ce 3d and (B) O 1s XPS spectra of $\text{Cr}_{0.19}\text{Rh}_{0.06}\text{CeO}_z$.	S11
Fig. S6. (A) k^3 -weighted Rh K-edge EXAFS oscillations and (B) their Fourier transforms ($k = 30\text{--}140\text{ nm}^{-1}$) for $\text{Cr}_{0.19}\text{Rh}_{0.06}\text{CeO}_z$ (a) during H_2 reduction at 330 K, (b) during H_2 reduction at 334 K, (c) before O_2 introduction at 303 K, and (d) after O_2 introduction at 303 K.	S12
Fig. S7. Setup for TPR/TPO measurements.	S13
Fig. S8. Setup for <i>in situ</i> QXAFS measurements.	S13
Fig. S9. Setup for CO oxidation.	S14
Scheme S1. Temperature-time protocol for <i>in situ</i> QXAFS measurements.	S14
References	S15

Details for catalyst characterization

Inductively coupled plasma atomic emission spectrometry (ICP-AES): The atomic compositions of samples were analyzed by ICP-AES (Vista-Pro-AX, Varian). Oxide samples were treated with fuming nitric acid at 353 K until solids were completely dissolved. The solutions were diluted with distilled water and filtered with a syringe filter (pore size: 0.2 $\mu\text{m}\phi$) prior to ICP-AES analysis. The atomic ratios of Ce, Cr, and Rh were estimated from the calibration curve prepared from standard solutions.

Brunauer-Emmett-Teller (BET) analysis: Nitrogen adsorption was performed on a surface adsorption analyzer (Micromeritics ASAP-2020, Shimadzu) at 77 K. Each sample (100–480 mg) was degassed at 423 K for 2 h under vacuum before the adsorption measurement. The dead volume was measured with helium after degassing before the adsorption measurement.

Powder X-ray diffraction (XRD): XRD patterns were recorded on an X-ray diffractometer (MultiFlex, Rigaku; Cu K_{α} , $\lambda = 1.5418 \text{ \AA}$, 40 kV, 30 mA) at a scan rate of $2^{\circ} \text{ min}^{-1}$ at 293–298 K under air. Commercial Cr_2O_3 (Sigma-Aldrich), CrO_3 (Wako), and Rh_2O_3 (Soekawa) were used for comparison.

Transmission electron microscopy (TEM) and high-angle annular dark field-scanning transmission electron microscopy (HAADF-STEM) with energy dispersive X-ray spectroscopy (EDS) and electron energy loss spectroscopy (EELS): TEM and HAADF-STEM images with EDS and EELS spectra were taken using a transmission electron microscope (JEM-ARM 200F, JEOL; accelerating voltage of 200 kV) at the High Voltage Electron Microscope Laboratory, Institute of Materials and Systems for Sustainability, Nagoya University, Japan. The sample was deposited directly on a Cu microgrid and was blown with an air duster gun to remove excess particles.

X-ray photoelectron spectroscopy (XPS): XPS was performed on X-ray photoelectron spectrometers: (ECSA3057, ULVAC PHI, base pressure: $1 \times 10^{-7} \text{ Pa}$, the X-ray source and power: Al K_{α} (1486.7 eV) and 350 W, pass energy: 11.75 eV, step size of 0.1 eV, a charge neutralization function was used to compensate for charge built up on the solid samples by X-ray irradiation) and (R4000, Scienta Omicron, base pressure: $1 \times 10^{-7} \text{ Pa}$, the X-ray source and power: Al K_{α} (1486.7 eV) and 180 W, pass energy: 200 eV, step size of 0.1 eV). The samples were ground and pressed into pellet disks (10 mm ϕ , 40 mg, pressed at 18 MPa), which were attached to the cell holder using carbon tape. The Shirley background was subtracted, and each peak was fitted by Voigt function. The binding energies were referenced to the O 1s peak of CeO_2 lattice oxygen (529.6 eV).

X-ray absorption fine structure (XAFS): XAFS spectra at the Cr K-edge and Ce L_{III}-edge were measured in transmission mode at room temperature at the BL9C and BL12C stations of the Photon Factory at KEK-IMSS (Tsukuba, Japan). The energy and current of the electrons in the storage ring were 2.5 GeV and 450 mA, respectively. X-rays from the storage ring were monochromatized with a Si(111) double-crystal monochromator. Two ionization chambers filled with a mixture of N_2 and He gases (3/7, v/v) and a mixture of N_2 and Ar gases (8.5/1.5, v/v) were used to monitor the incident (I_0) and transmitted (I) X-rays, respectively. CeO_2 , $\text{Ce}_2(\text{CO}_3)_3$, Cr_2O_3 , $\text{Cr}(\text{OH})_3$, CrO_3 (diluted with boron nitride), and Cr foil were used as references.

XAFS spectra at the Rh K-edge were measured in transmission mode at room temperature at the NW10A stations of the Photon Factory at KEK-IMSS. The energy and current of the electrons in the storage

ring were 6.5 GeV and 60 mA, respectively. X-rays from the storage ring were monochromatized with a Si(311) double-crystal monochromator. Two ionization chambers filled with pure Ar and Kr gases were used to monitor the incident (I_0) and transmitted (I) X-rays, respectively. Rh foil and Rh₂O₃ (diluted with boron nitride) were used as references.

The XAFS spectra were analyzed using ATHENA and ARTEMIS with IFEFFIT (version 1.2.11).¹ The threshold energy was tentatively set at the inflection point for the Cr K-edge (Cr foil: 5988.8 eV)² and Rh K-edge (Rh foil: 23219.8 eV),² and at the first peak top of the white line for the Ce L_{III}-edge (CeO₂: 5734.4 eV). Background subtraction was performed using the Autobk method and the spline smoothing algorithm in ATHENA.³ The average oxidation states of Ce, Cr, and Rh were determined from the changes at 5741.3 eV (second peak top of the white line), 5991.4 eV (pre-edge), and 23238 eV (white line peak top), respectively. The k^3 -weighted extended XAFS (EXAFS) oscillations were Fourier transformed into R -space. Curve-fitting analysis was carried out in the R -space. The fitting parameters for each shell were the coordination number (CN), interatomic distance (R), Debye–Waller factor (σ^2 : mean-square displacement), and correction-of-edge energy (ΔE_0). For the Rh K-edge, S_0^2 was fixed to be 1 based on the fitting of Rh foil, and S_0^2 for Rh₂O₃ was fitted to be 0.92, which was rounded to 1. Phase shifts and backscattering amplitudes for Rh-O and Rh-Rh were calculated with FEFF 8 code⁴ using structural parameters obtained from the crystal structures of Rh^{5a} and Rh₂O₃.^{5b}

Table S1. Catalytic Performances for 1-Octanol Oxidation^a

Catalyst	Atmosphere	Initial reaction rate	Yield % ^c
		/mol g _{cat} ⁻¹ min ⁻¹ ^b	6 h / 24 h
(Blank) ^d	O ₂	---	0.0 / 0.0
Cr _{0.19} Rh _{0.06} CeO _z	N ₂	2.1×10 ⁻⁵	4.3 / 4.4
Cr _{0.19} Rh _{0.06} CeO _z	O ₂	2.5×10 ⁻⁵	7.9 / 9.8
(recycled, filtered catalyst)	O ₂	---	0.6 / 2.0
(recycled, calcined catalyst)	O ₂	2.5×10 ⁻⁵	7.5 / 9.8
CeO ₂ ^e	O ₂	~ 0	0.1 / 0.9
Cr _{0.17} CeO _z ^f	O ₂	1.7×10 ⁻⁵	5.4 / 7.5
Rh _{0.04} CeO _z ^g	O ₂	3.2×10 ⁻⁶	1.1 / 1.6

^a Reaction conditions: catalyst, 150 mg; Rh/Cr/1-octanol/dodecane (internal standard), 1/3/100/50; 1-octanol, 0.42 mol L⁻¹ in toluene; 343 K, atmospheric pressure.

^b Initial reaction rate (mol (*n*-octanal) g_{cat}⁻¹ min⁻¹) = (change in the mol of *n*-octanal between 0-60 min. /mol min⁻¹) / (the amount of catalyst /g).

^c Yield (%) = (amount of *n*-octanal/amount of dodecane × 2) × 100.

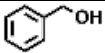
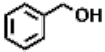
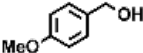
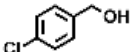
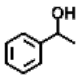

^d A blank test was performed in the absence of catalyst. Reaction conditions: 1-octanol/dodecane, 100/50; 1-octanol, 0.42 mol L⁻¹; toluene, 2 mL. The reaction was performed in a Schlenk tube with a balloon of O₂.

^e Reaction conditions: CeO₂, 150 mg; 1-octanol/dodecane, 100/50; 1-octanol, 0.42 mol L⁻¹; toluene, 10 mL.

^f Reaction conditions: catalyst, 151 mg; Cr/1-octanol/dodecane, 3/100/50; 1-octanol, 0.42 mol L⁻¹; toluene, 10 mL.

^g Reaction conditions: catalyst, 150 mg; Rh/1-octanol/dodecane, 1/108/54; 1-octanol, 0.42 mol L⁻¹; toluene, 10 mL.

Table S2. Catalytic Performances of Cr_{0.19}Rh_{0.06}CeO_z for the Selective Oxidation of Alcohols^a

Entry	Reactant	Atmosphere	Yield % ^b
			6 h / 24 h
1		O ₂	21 / 28
2		N ₂	4.3 / 6.2
3		O ₂	27 / 33
4		O ₂	15 / 23
5		O ₂	32 / 47
6		O ₂	1.8 / 2.7

^a Reaction conditions: catalyst, 150 mg; Rh/Cr/alcohol/dodecane (internal standard), 1/3/100/50; 0.42 mol L⁻¹ of alcohol in toluene; temperature, 343 K; atmospheric pressure.

^b Yield (%) = (amount of product/amount of dodecane × 2) × 100.

Table S3. Structural Parameters Obtained by Curve-Fitting Analysis of Rh K-edge EXAFS for $\text{Cr}_{0.19}\text{Rh}_{0.06}\text{CeO}_z$ ^a

Shell	CN	R/nm	$\Delta E_0/\text{eV}$	$\sigma^2/10^5 \text{ nm}^2$
During H₂ reduction (330 K) ^b				
Rh–O	5.8 ± 1.3	0.204 ± 0.001	11 ± 2	5 ± 2
During H₂ reduction (334 K) ^c				
Rh–O	2.8 ± 0.3	0.205 ± 0.002	9 ± 2	4 ± 1
Rh–Rh	2.6 ± 0.7	0.270 ± 0.002	4 ± 2	10 ± 2
Before O₂ introduction (303 K) ^d				
Rh–O	1.8 ± 0.3	0.206 ± 0.003	9 ± 2	4 ± 1
Rh–Rh	3.1 ± 0.5	0.269 ± 0.001	2 ± 1	9 ± 1
After O₂ introduction (303 K) ^e				
Rh–O	5.8 ± 1.6	0.204 ± 0.001	11 ± 2	6 ± 3

^a $k = 30\text{--}140 \text{ nm}^{-1}$, S_0^2 was fixed as 1. ^b $R = 0.12\text{--}0.20 \text{ nm}$, $R_f = 0.9\%$. ^c $R = 0.12\text{--}0.27 \text{ nm}$, $R_f = 0.5\%$. ^d $R = 0.12\text{--}0.27 \text{ nm}$, $R_f = 0.4\%$. ^e $R = 0.12\text{--}0.20 \text{ nm}$, $R_f = 1.6\%$.

Table S4. Parameters for *In Situ* QXAFS Measurements

Edge	Energy range /eV	Scan time /s	Scan interval /s	Data Points
Ce L _{III}	5670-5820	10	15	300
Cr K	5950-6100	10	15	303
Rh K	22900-24300	55	60	1422

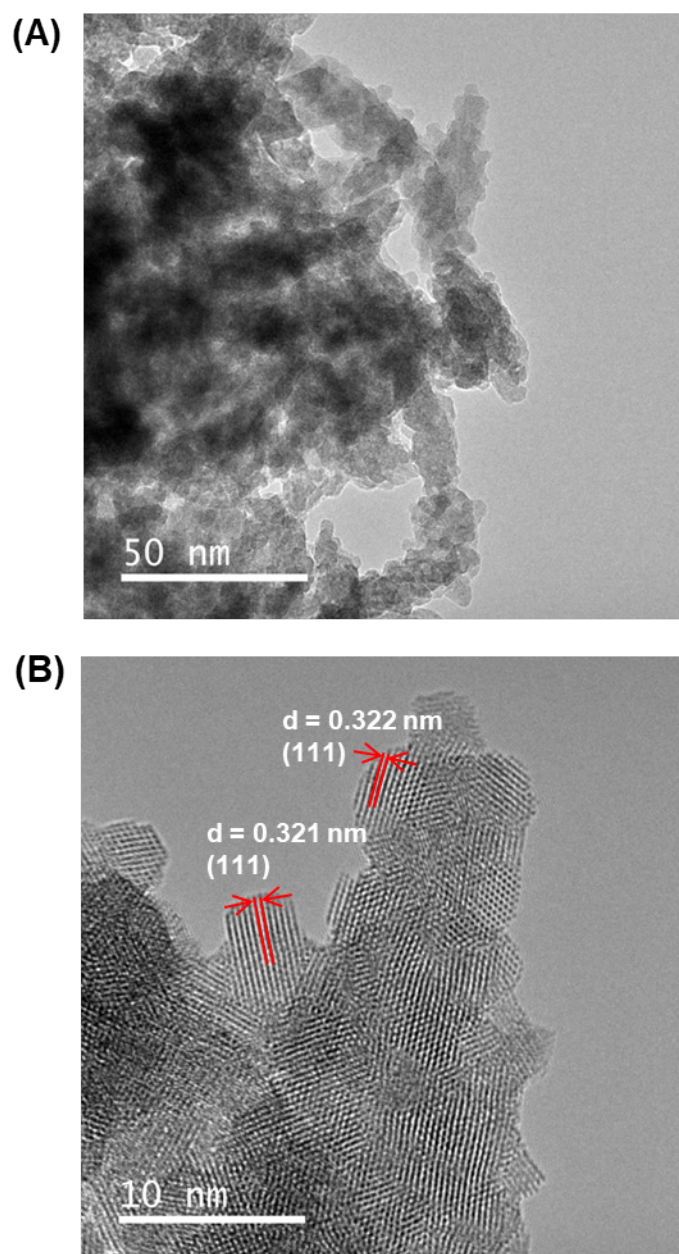


Fig. S1. TEM images of $\text{Cr}_{0.19}\text{Rh}_{0.06}\text{CeO}_z$.

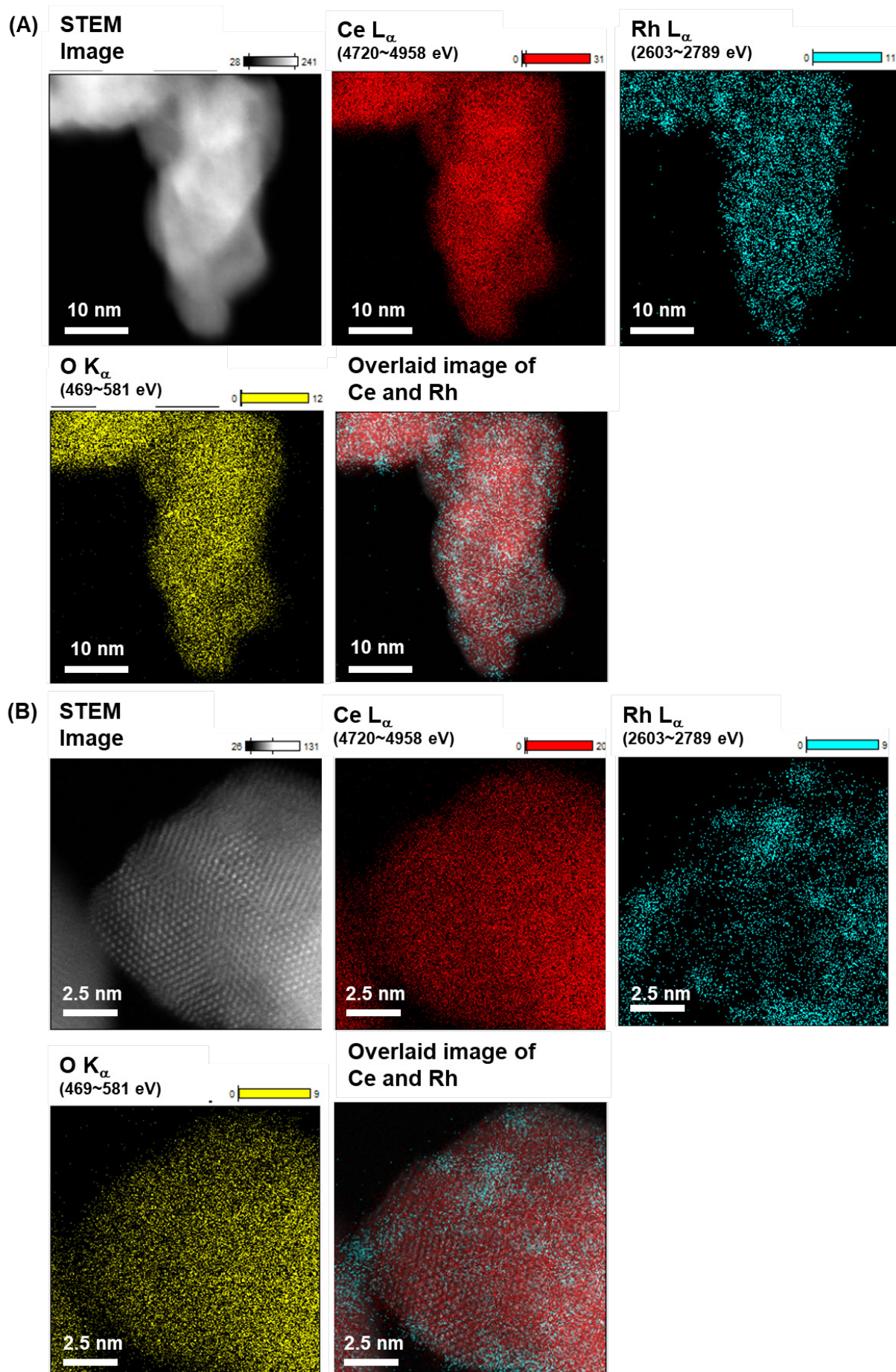


Fig. S2. HAADF-STEM-EDS images of $\text{Cr}_{0.19}\text{Rh}_{0.06}\text{CeO}_z$.

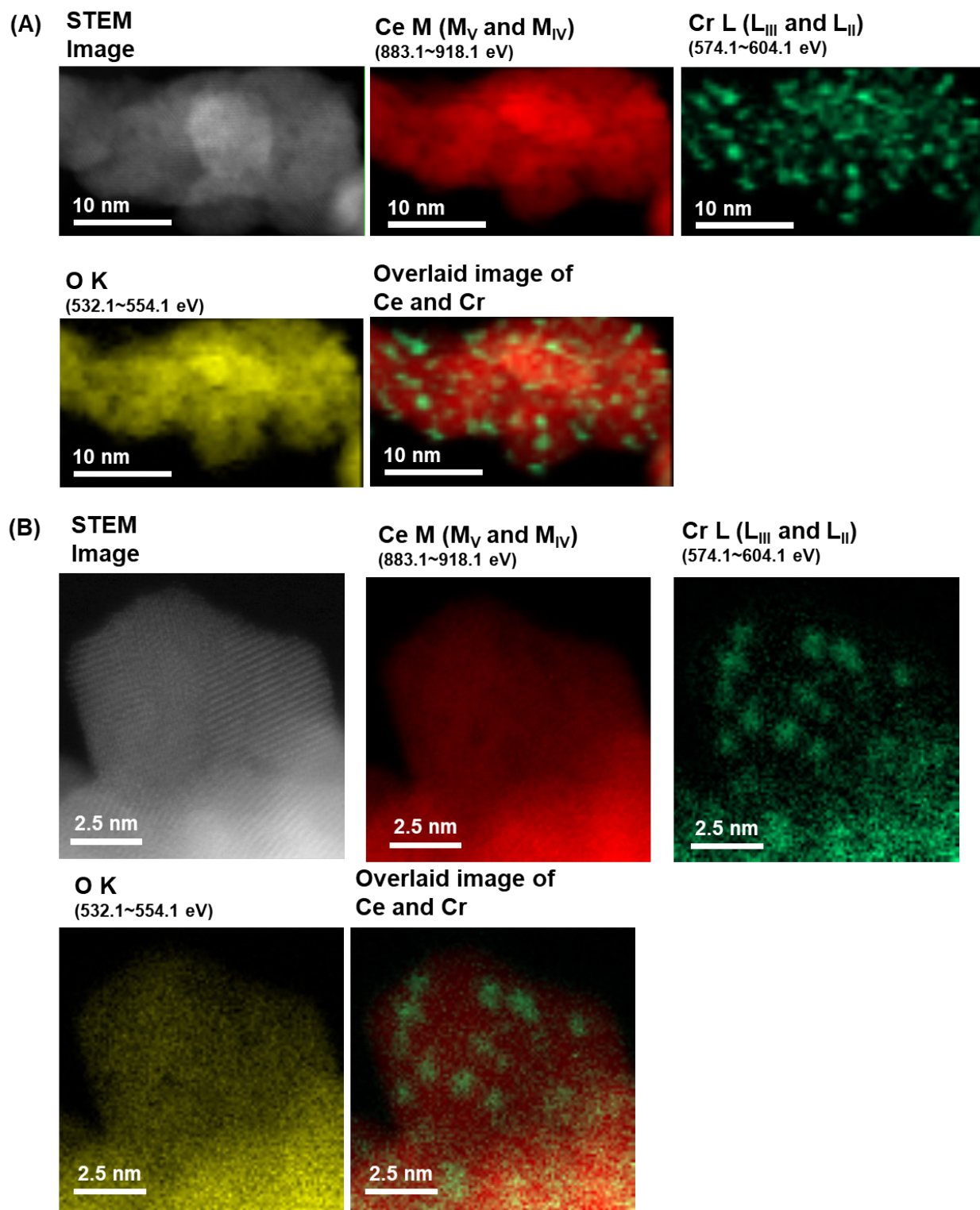


Fig. S3. HAADF-STEM-EELS images of $\text{Cr}_{0.19}\text{Rh}_{0.06}\text{CeO}_z$.

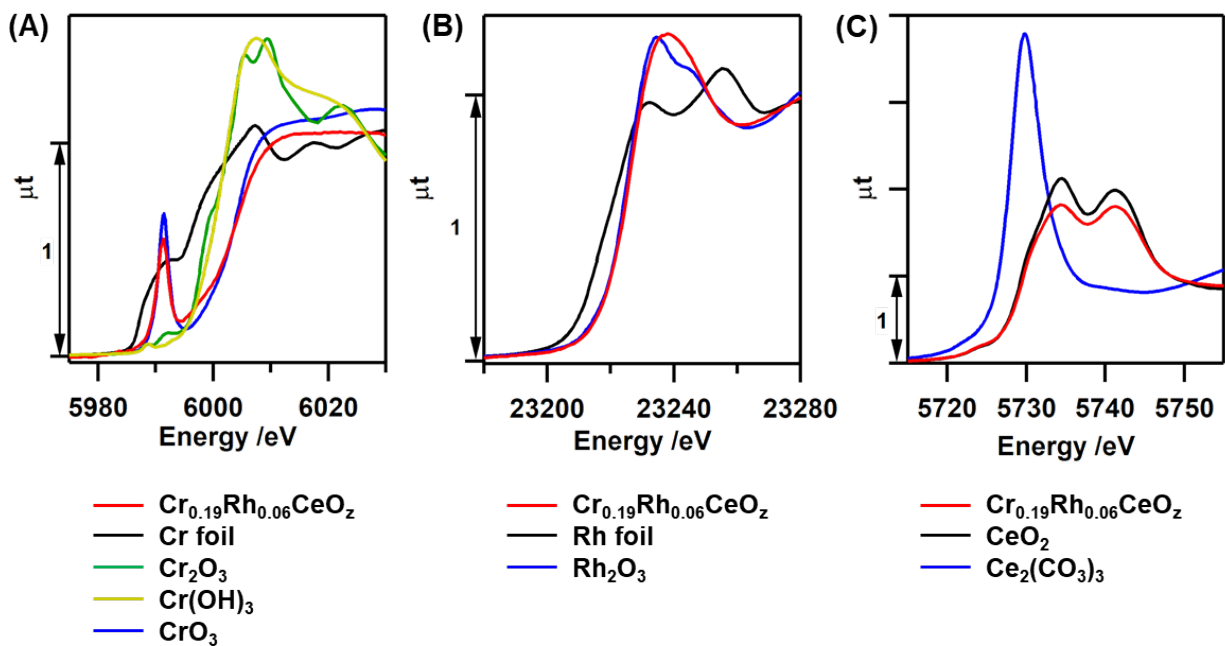


Fig. S4. (A) Cr K-edge, (B) Rh K-edge, and (C) Ce L_{III}-edge XANES spectra of $\text{Cr}_{0.19}\text{Rh}_{0.06}\text{CeO}_z$ with standard samples.

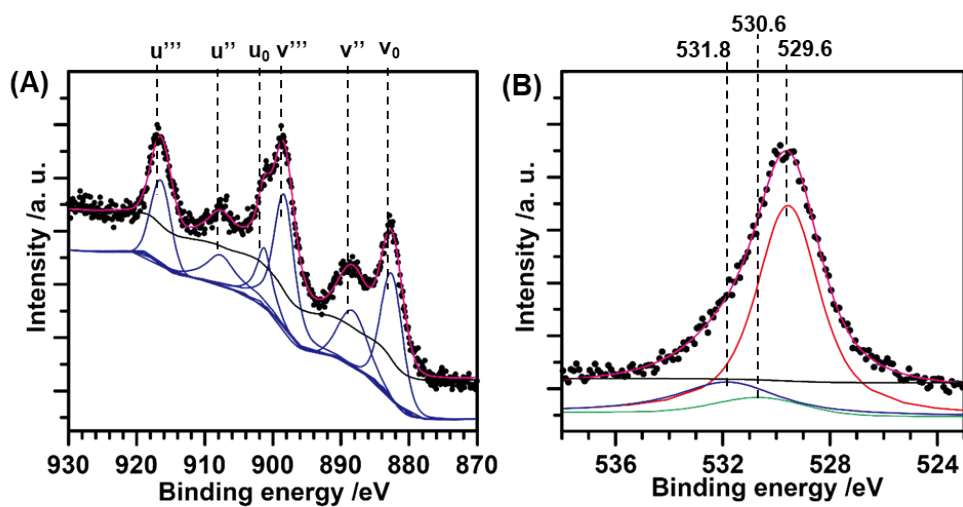


Fig. S5. (A) Ce 3d and (B) O 1s XPS spectra of $\text{Cr}_{0.19}\text{Rh}_{0.06}\text{CeO}_z$.

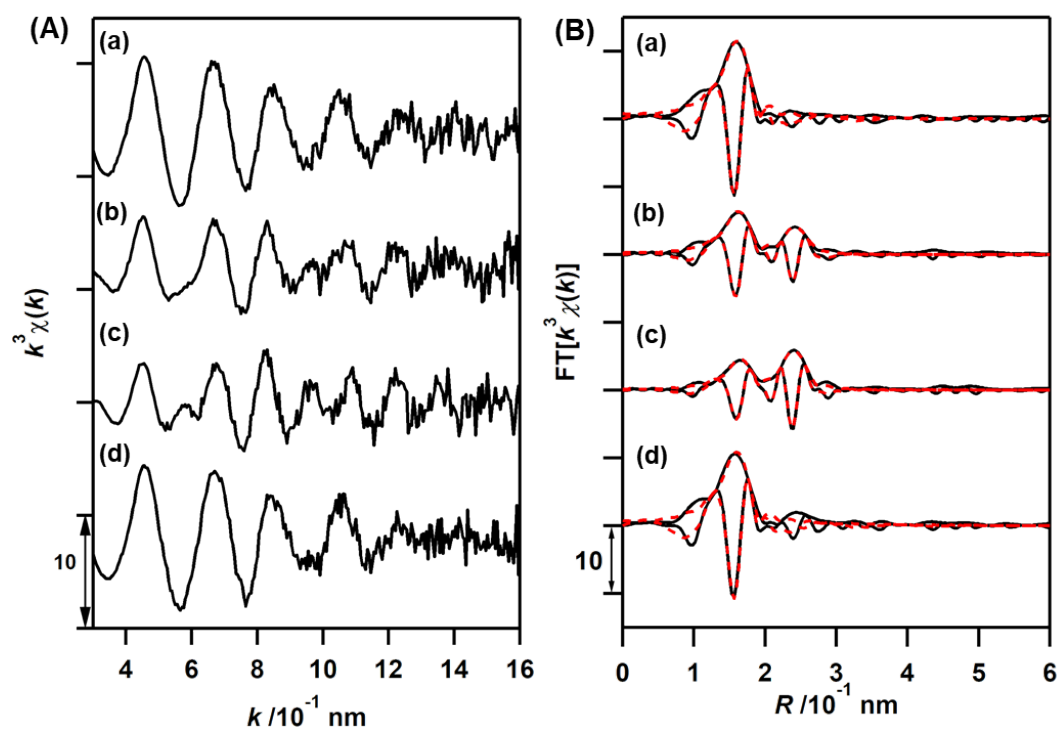


Fig. S6. (A) k^3 -weighted Rh K-edge EXAFS oscillations, and (B) their Fourier transforms ($k = 30\text{--}140 \text{ nm}^{-1}$) for $\text{Cr}_{0.19}\text{Rh}_{0.06}\text{CeO}_x$ (a) during H_2 reduction at 330 K, (b) during H_2 reduction at 334 K, (c) before O_2 introduction at 303 K, and (d) after O_2 introduction at 303 K. Black solid lines in (B) show observed data and red dashed lines show fitted data.

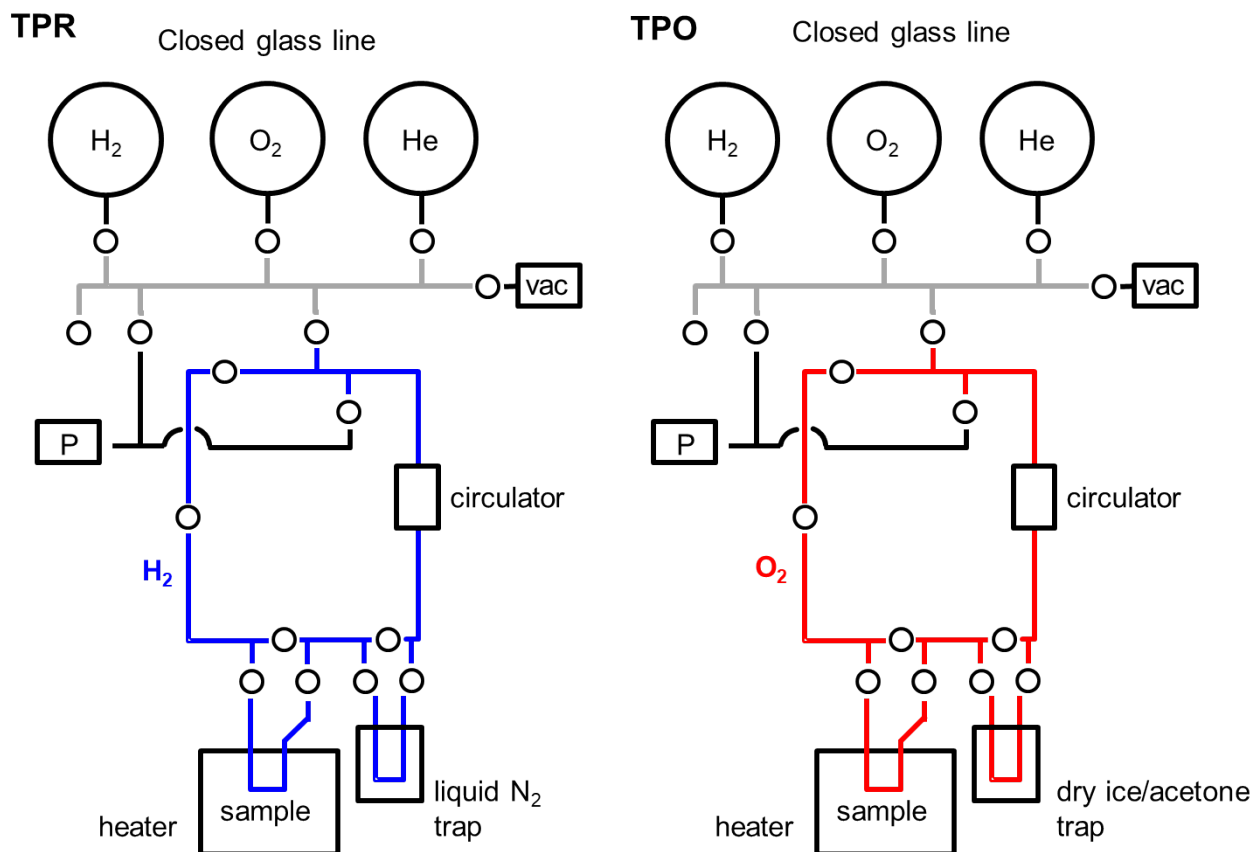


Fig. S7. Setup for TPR/TPO measurements.

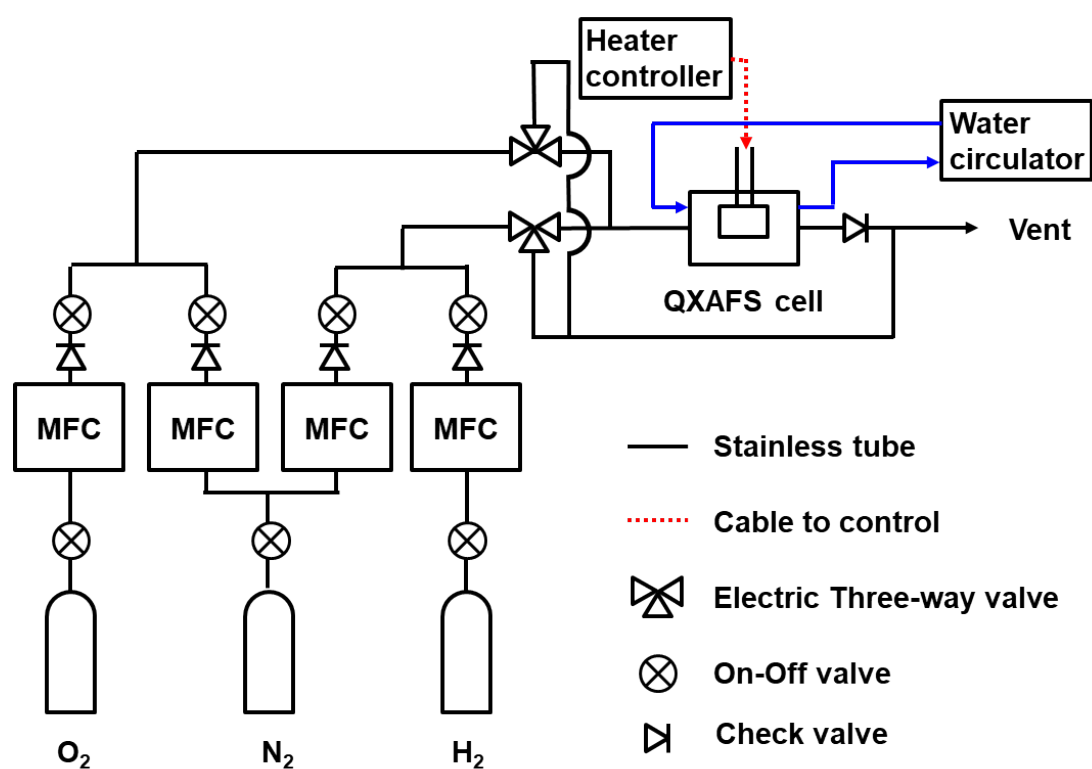
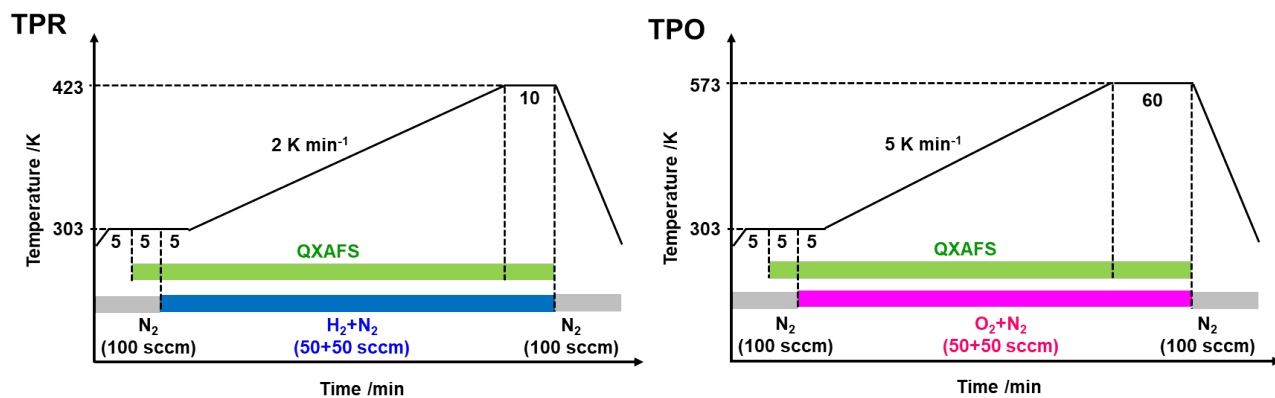


Fig. S8. Setup for *in situ* QXAFS measurements.



Scheme S1. Temperature-time protocol for *in situ* QXAFS measurements.

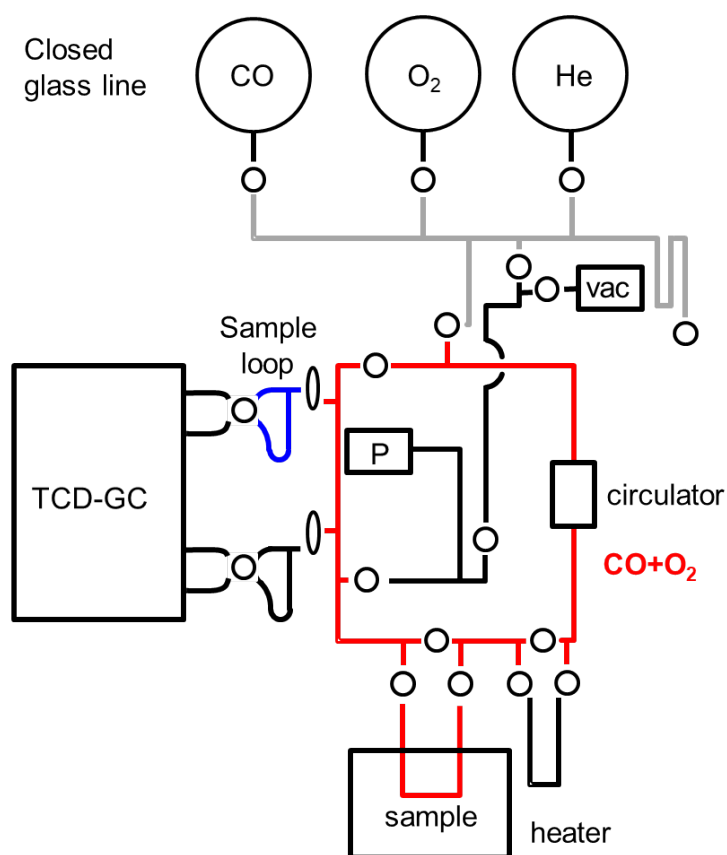


Fig. S9. Setup for CO oxidation.

References

- (1) (a) B. Ravel, M. Newville, *J. Synchrotron Rad.* 2005, **12**, 537–541. (b) M. Newville, B. Ravel, D. Haskel, J. J. Rehr, E. A. Stern, Y. Yacoby, *Physica B* 1995, **208-209**, 154–156.
- (2) J. A. Bearden, A. F. Burr, *Rev. Mod. Phys.* 1967, **39**, 125–142.
- (3) (a) M. Newville, *J. Synchrotron Rad.* 2001, **8**, 322–324. (b) M. Newville, P. Līviņš, Y. Yacoby, J. J. Rehr, E. A. Stern, *Phys. Rev. B* 1993, **47**, 14126–14131.
- (4) A. L. Ankudinov, B. Ravel, J. J. Rehr, S. D. Conradson, *Phys. Rev. B* 1998, **58**, 7565–7576.
- (5) (a) H. E. Swanson, G. M. Ugrinic, *National Bureau of Standards Circular (U. S.)*, 1954, **539**, 1–75. (b) J. M. D. Coey, *Acta Crystallogr., B* 1970, **26**, 1876–1877.